

SPARSE SAMPLING FOR SOFTWARE DEFINED RADIO RECEIVERS

*F. Palmieri #, E. Venosa #, A. Petropulu *, G. Romano #, P. Salvo Rossi #*

Dipartimento di Ingegneria dell'Informazione,
Seconda Università degli Studi di Napoli,
Via Roma, 29, 81031 Aversa (CE), Italy.

* Electrical and Computer Engineering Department,
Drexel University,
3141 Chestnut Street, Philadelphia, PA 19104, USA.

ABSTRACT

In this paper we address the problem of designing a back-end for Software Defined Radio (SDR) receiver using only one low-rate Analog-to-Digital Converter (ADC). After the Intermediate Frequency (IF) down-conversion stage, the signals are sampled and all the other demodulation tasks are assigned to a Digital Signal Processor (DSP). In this paper we concentrate on only one Quadrature Amplitude Modulation (QAM) signal. After reduction of the communication chain to a linear model, the issue of proper sampling rate choice is addressed. It is shown how improper sampling rate can lead to a poorly conditioned problem that causes symbol cancellations and poor performances. In the analysis the role of the device noise at the input of the ADC is also addressed by computing autocorrelation and Power Spectral Density (PSD) after undersampling. Some simulations confirm the analysis.

1. INTRODUCTION

Software Defined Radio is one of the most important emerging technologies for the future of the communication systems. By moving radio functionalities into software, SDR promises to change the structure of the radio receivers making them extremely flexible, reconfigurable and reprogrammable [1], [2], [3]. Traditional designs implementing the conventional digital receiver architectures are usually optimized for specific center frequencies and bandwidths. Therefore, in many applications that require multiple stages to be implemented in analog hardware, the receivers may not be very flexible, since the various blocks may be closely coupled [14].

If we were able to move the ADC closer to receiver antenna [1], [2], many of the demodulation tasks could be assigned to numerical algorithms. Nevertheless, moving the ADC closer to receiver antennas would imply using highest frequencies to sample incoming signals because Nyquist's sampling theorem prescribes a minimum sampling rate that is twice the maximum signal frequency [6], [7], [8]. Hence, when following the standard Low-Pass Sampling (LPS) theory, the ADC, must work at very high rates and sort among very large amounts of data. This is highly redundant because the information rate contained in the received signal is related to its bandwidth rather than to its largest frequency [2] and it should be possible to use undersampling techniques [4], [5]. More specifically, if the signal is limited to a given frequency interval, the theory predicts that we can sample the received signal with a sampling rate smaller than twice the maximum frequency and larger than twice the bandwidth, but not all sampling rates in this range are allowed. Special attention should

be paid to appropriate rate selection to avoid symbol cancellations as a consequence of spectral overlaps (aliasing). Sampling directly the IF signals poses also technology challenges in designing chips for ADC [9], [10]. Many authors are trying to extend the capabilities of ADCs by investigating new approaches and methods that increase sensitivity and resolution [11], [12].

In addition to proper rate selection, a technical difficulty that limits the use of direct sampling is the noise coming from the ADC: even if the converter samples at low rate, it must "see" a large input bandwidth that causes device noise to enter the system. Device producers are currently working to supply the market with ADCs that have larger bandwidths with good noise figures.

In this paper we address both the above mentioned issues as they are reflected in receiver design and performance with reference to a QAM signal. More specifically we investigate:

1. Appropriate sampling rate selection;
2. ADC noise modeling.

In Section 2 we introduce the problem and reduce the communication chain to a linear model. After the application of an alias-free conditions, we demonstrate how poorly chosen sampling rates can make the linear problem ill-conditioned. The alias-free condition that we use here is a generalization of the band-pass sampling theorem [4], and can be applied to multi-band signals [15], even though we confine ourselves in this paper to one-band cases. Particular attention is also dedicated to the noise aliasing problem. We derive the autocorrelation and the PSD caused by the devices noise in the numerical frequency domain. In Section 3 we discuss the receiver design while in Section 4 we report some simulations in terms of Bit Error Rate (BER) for different sampling rates and receivers.

2. DIRECT SAMPLING AND NOISE ALIASING

The classical structure of a QAM digital receiver is based on the cascade of a down-conversion stages, that shifts the signal to an intermediate frequency, and two Analog-to-Digital Converters whose output samples are processed by a Digital Signal Processor for symbol recovery [14]. In this paper we explore the possibility of using low-rate sampling with only one ADC, as shown in Fig. 1 [3],[2].

The QAM signal is written as

$$y(t) = z(t) + w_g(t) = \sum_{i=1}^L [I_i \psi_c(t; i) - Q_i \psi_s(t; i)] + w_g(t) \quad (1)$$

with $\psi_c(t; i) = \cos(2\pi f_0 t)g(t - iT_s)$, $\psi_s(t; i) = \sin(2\pi f_0 t)g(t - iT_s)$ and $g(t)$ is the equivalent pulse that includes the transmitted waveform, the channel and the receiver input filter; (I_i, Q_i) , $i = 1, \dots, L$ is the sequence of L modulating pairs (symbols), f_0 is the carrier frequency after intermediate frequency shifting, T_s is the symbol time, and $w_g(t)$ is Additive White Gaussian Noise (AWGN). For applying direct low-rate sampling to this signal,

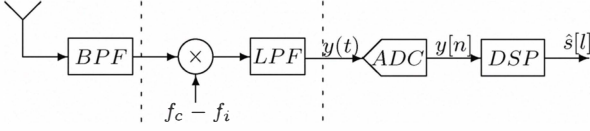


Fig. 1. Digital receiver with direct low-rate sampling.

along with choosing the appropriate sampling rate, we have to account for the effects of ADC, that unfortunately result in extra noise into the receiver, as shown in the simplified model of Fig. 2. The low-pass filter at the input of the ADC must have a very large analog band, $\mathcal{B}_{ADC} = [-f_{ADC}, f_{ADC}]$, sufficient to contain frequencies up to the maximum frequency of the incoming signal. In fact, even if the information signal is limited to a narrow band, the sampler that works at low-rate on a high-frequency signal must have a sufficient time resolution to capture the fine signal details. Therefore, such an “open band” at the input causes extra noise to enter the receiver. After low-rate sampling, and consequent spectral folding, ADC noise can become a penalizing factor in receiver performance.

Modeling the ADC as in Fig. 2 and after ideal sampling at time $t_n = nT_{SA} + t_0$, we get at the output

$$y[n] = \sum_{i=1}^L [I_i \psi_c(nT_{SA} + t_0; i) - Q_i \psi_s(nT_{SA} + t_0; i)] + w_g(nT_{SA} + t_0) + w_{ADC}(nT_{SA} + t_0). \quad (2)$$

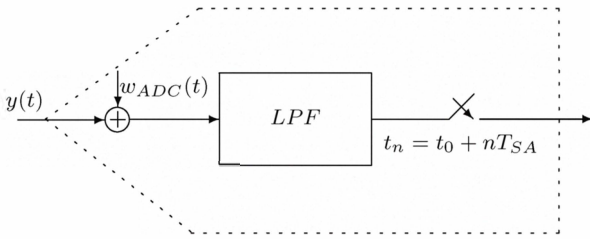


Fig. 2. Model of the ADC with the device noise.

Gathering N values in a vector $\mathbf{y} = [y[1] \dots y[N]]^T$, the system is reduced to the linear model

$$\mathbf{y} = \mathbf{C}\mathbf{s} + \mathbf{w}_g + \mathbf{w}_{ADC} \quad (3)$$

where $\mathbf{s} = [I_1 \ Q_1 \ I_2 \ Q_2 \dots \ I_L \ Q_L]^T$,

$$\mathbf{C} = \begin{pmatrix} \psi_c[1; 1] & \psi_c[2; 1] & \dots & \psi_c[N; 1] \\ \psi_s[1; 1] & \psi_s[2; 1] & \dots & \psi_s[N; 1] \\ \psi_c[1; 2] & \psi_c[2; 2] & \dots & \psi_c[N; 2] \\ \psi_s[1; 2] & \psi_s[2; 2] & \dots & \psi_s[N; 2] \\ \dots & \dots & \dots & \dots \\ \psi_c[1; L] & \psi_c[2; L] & \dots & \psi_c[N; L] \\ \psi_s[1; L] & \psi_s[2; L] & \dots & \psi_s[N; L] \end{pmatrix}^T$$

$\psi_c[n; i] = \psi_c(nT_s + t_0; i)$, $\psi_s[n; i] = \psi_s(nT_s + t_0; i)$, $n = 1, \dots, N$, $i = 1, \dots, L$. \mathbf{w}_g is the noise contribution from the channel, it is Gaussian with zero mean and $cov[\mathbf{w}_g] = \sigma_g^2 \mathbf{I}_M$ while \mathbf{w}_{ADC} is the contribution from the ADC noise (to be discussed later). We have in total L symbols, but we take $n = 1, \dots, N$ samples to include most of the pulse waveforms by choosing initial time $t_0 = -L_e + 1$ and $N = \lceil \frac{(L+2L_e)T_s}{T_{SA}} \rceil$. This includes about L_e extra symbol intervals on the left and L_e on the right. Matrix \mathbf{C}^T contains in its rows the bases on which the information vector \mathbf{s} is projected. Since no constraints on symbol time and sampling frequencies are imposed, sampling and symbol timing can be totally asynchronous. Therefore subsequent pairs of rows of \mathbf{C}^T are not shifted versions of each other. In a vector space framework, the bases do not necessarily form a shift-invariant subspace [5]. Figure 3 shows an example with

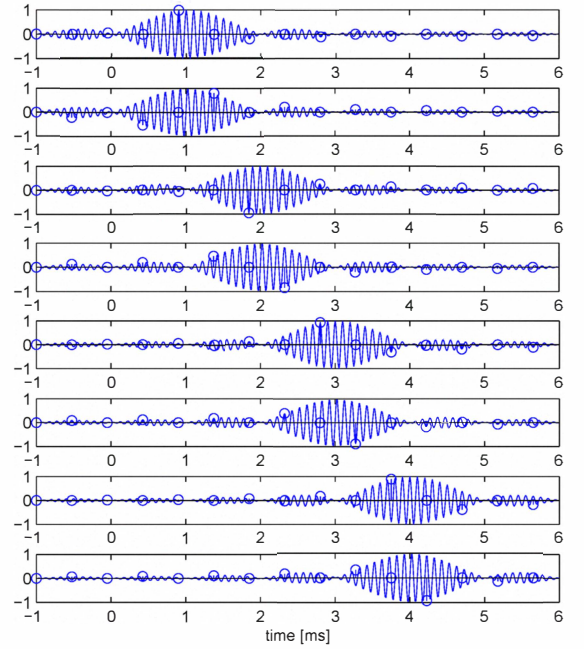


Fig. 3. Sampling bases for $g(t) = \text{sinc}(\frac{t}{T_s})$, with $T_s = 1 \times 10^{-3} s$, $t_0 = 0.01 \times 10^{-3} s$, $T_{SA} = 0.475 \times 10^{-3} s$, $f_0 = 10 \text{ KHz}$, $L = 4$ and $L_e = 2$.

$L = 4$. Note how sparse sampling produces varying patterns that may become critical if some sample values become too small.

2.1. Sampling Rate Selection

The first problem to solve in designing a receiver with direct low-rate sampling is the selection of the sampling frequency. It is often mistakenly assumed that the minimum sampling rate is twice the signal bandwidth. The data-rate in the signal is only one sample per symbol, and that would suggest that sampling at the baudrate should ideally resolve all the degrees of freedom. Unfortunately this is an asymptotic result (Landau's rate) [5][7]. Various contributions have appeared in the literature proposing alternate sampling schemes [5] in trying to reach Landau's rate. However, in the framework of Fig. 1, we are confined to uniform sampling, and not all sampling rates are allowed. Poor decoding performance and symbol erasures can occur because the linear problem (3) can become ill-conditioned.

It is shown in the Appendix that if N is sufficiently large, there is no degeneracy, or loss of information after sampling if the following alias-free condition is satisfied

$$\mathcal{F} [|\psi_c(t) + \psi_s(t)|^2] \Big|_{f=mf_{SA}} = 0 \quad \forall m \neq 0 \quad (4)$$

where $\psi_c(t) = \psi_c(t; 0)$, $\psi_s(t) = \psi_s(t; 0)$ and $\mathcal{F}[\cdot]$ denotes the Fourier transform. The criterion can be easily applied if ψ_c and ψ_s are bandlimited and occupy the same band $\mathcal{B} = [-f_u, -f_l] \cup [f_l, f_u] = [-f_0 - \frac{W}{2}, -f_0 + \frac{W}{2}] \cup [f_0 - \frac{W}{2}, f_0 + \frac{W}{2}]$. By defining an indicator function $I(f) = 1, f \in \mathcal{B}, = 0$ else, Eq. (4) can be rewritten as

$$\int_{-\infty}^{\infty} I(f)I(f - mf_{SA})df = (I * I)(f) \Big|_{f=mf_{SA}} = 0 \quad \forall m \neq 0 \quad (5)$$

where $*$ denotes the convolution. Condition (5), based on indicator functions is a special case of a condition derived in [13] within the context of multi-dimensional lattices. In this paper we focus on only one QAM signal, but a generalization of Eq. (4) can be applied to multiple superimposed signals [15].

With a QAM signal, that is exactly limited to one band, the alias-free condition reduces to check if frequencies $f = mf_{SA}, m \neq 0$ intersect the set $\mathcal{B}_{\frac{1}{2}} = [-2f_u, -2f_l] \cup [-W, W] \cup [2f_l, 2f_u]$. No aliasing occurs if $2f_u \leq f_{SA} \leq \infty$ (Nyquist rate), $\frac{2f_u}{2} \leq f_{SA} \leq 2f_l$, $\frac{2f_u}{3} \leq f_{SA} \leq \frac{2f_l}{2}$ until $\frac{2f_u}{k} \leq f_{SA} \leq \frac{2f_l}{k-1}$ with $1 \leq k \leq \lfloor \frac{f_u}{W} \rfloor$. These are the results found on the classical band-pass sampling theorem [4].

After sampling, the signal spectrum will be still symmetric around the zero frequency, but not exactly centered on it. In the normalized frequency $\nu = f/f_{SA}$ domain, the signal will be centered at ν_0 and occupy the range $[-\nu_u, -\nu_l] \cup [\nu_l, \nu_u]$ where $\nu_0 = \frac{f_0}{f_{SA}} - \frac{k-1}{2}$,

$$[\nu_l, \nu_u] = \left[\frac{f_l}{f_{SA}} - \frac{k-1}{2}, \frac{f_u}{f_{SA}} - \frac{k-1}{2} \right], \quad (6)$$

for k odd, and $\nu_0 = -\frac{f_0}{f_{SA}} + \frac{k}{2}$,

$$[\nu_l, \nu_u] = \left[-\frac{f_u}{f_{SA}} + \frac{k}{2}, -\frac{f_l}{f_{SA}} + \frac{k}{2} \right], \quad (7)$$

for k even. In the latter case with k even, the digital spectrum has the upper and the lower side-bands inverted.

Note that in the linear model of Eq. (3), N increases with the sampling rate. We assume that $M = 2L$ is kept smaller or equal to N , i.e. at any rate we gather enough samples to make the linear model *overdetermined* (the *underdetermined* problem with $M > N$ will be addressed elsewhere). Therefore, as the result of improper sampling, loss of rank of \mathbf{C} means that $\mathbf{C}^T \mathbf{C}$ can become singular.

Note that $\mathbf{C}^T \mathbf{C}$ contains in its diagonal the energies of all the basis vectors and the off-diagonal elements are all the cross products. The eigenvalue spread of $\mathbf{C}^T \mathbf{C}$ can tell us how critical the solution to the linear problem of Eq. (3) can become. Figure 4 shows a typical plot of the condition number in log scale for $\mathbf{C}^T \mathbf{C}$ at various sampling intervals for the example of Fig. 3. The signal occupies the band $[f_0 - \frac{1}{2T_s}, f_0 + \frac{1}{2T_s}] = [9.5, 10.5]KHz$ with $f_0 = 10KHz$. Nyquist's sampling rate would be $f_{SA} \geq 2f_u = 21KHz$, i.e. $T_{SA} \leq 0.0476 \times 10^{-3}s$. However, we see from Fig. 4 that sampling at lower rates is possible with favorable condition numbers, but not all sampling rates are allowed. Superimposed to the condition number plot is a square wave indicating the sampling intervals predicted by the alias-free condition (4). On the left-end we see the range with $T_{SA} \in [0, 0.0476] \times 10^{-3}s$ (Nyquist's rates). In the last allowed range $T_{SA} \in [0.4737, 0.4762] \times 10^{-3}s$ the value of N varies from 169 to 17. Therefore, at the lowest allowed sampling interval $N = 17 > M = 8$, i.e. the linear system remains overdetermined.

2.2. ADC Noise

To better understand the practical difficulties in applying low-rate sampling, we have considered also the model of the ADC shown in Fig. 2. As pointed out above, the input LPF must have $f_{ADC} \geq f_u$, and unfortunately, at the input of the ADC, the noise power, initially negligible (in power/Hz), increases with undersampling because of spectral folding (noise aliasing). Modeling the device noise as flat low-pass Gaussian noise with power spectral density $\frac{\eta_{ADC}}{2}$ and defining the ADC decimation factor as

$$K_{ADC} = \left\lfloor \frac{2f_{ADC}}{f_{SA}} \right\rfloor \geq 1 \quad (8)$$

we obtain the noise PSDs shown in Fig. 5 with

$$\begin{aligned} \nu_o &= \frac{K_{ADC}+1}{2} f_{SA} - f_{ADC}, \\ \nu_e &= -\frac{K_{ADC}}{2} f_{SA} + f_{ADC}. \end{aligned} \quad (9)$$

The autocorrelation of $w_{ADC}[n] = w_{ADC}(t_0 + nT_{SA})$ is

$$r_{ADC}[m] = \begin{cases} f_{SA}\eta_{ADC} \left(\frac{K_{ADC}}{2} \delta[m] + \nu_o \text{sinc} 2\nu_o m \right) \\ f_{SA}\eta_{ADC} \left(\frac{K_{ADC}+1}{2} \delta[m] - \nu_e \text{sinc} 2\nu_e m \right) \end{cases} \quad (10)$$

for K_{ADC} odd and even, respectively. From Eq. (10) we note that the noise aliasing is weakly correlated when K_{ADC} is large, i.e. $w_{ADC}[n]$ is almost white. In the frequency domain, as shown in Fig. 5 the steps on both PSDs differ slightly and become negligible as K_{ADC} grows. In the receiver design we assume that ADC noise is white and has variance $\sigma_{ADC}^2 = f_{SA}\eta_{ADC} \left(\frac{2K_{ADC}+1}{4} \right)$. Therefore we add the ADC noise to the channel noise into a Gaussian vector $\mathbf{w} = \mathbf{w}_c + \mathbf{w}_{ADC}$ with zero mean and covariance $\sigma_w^2 \mathbf{I}_M$, $\sigma_w^2 = \sigma_g^2 + \sigma_{ADC}^2$.

3. RECEIVER DESIGN

We consider now the standard solutions to the linear problem of Eq. (3) under the assumption of perfectly known \mathbf{C} and Signal-to-Noise Ratio (SNR), to verify the validity of the sampling criterion. Recall that sampling rate design requires only knowledge of the signal band. Therefore matrix \mathbf{C} , that includes also the channel, can be estimated with standard techniques using pilot symbols.

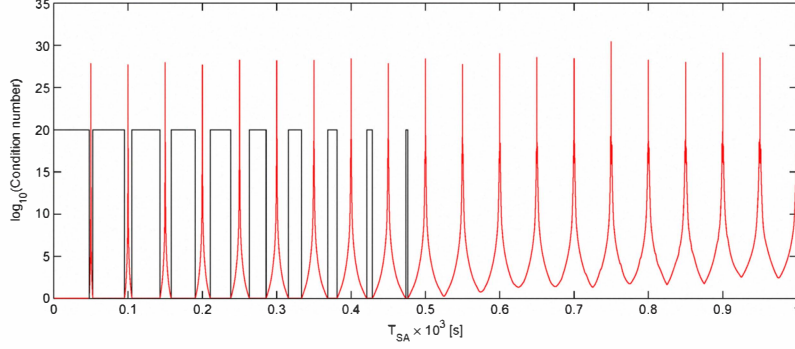


Fig. 4. Log-plot of the condition number of $\mathbf{C}^T \mathbf{C}$ for the example of Fig. 3 for various sampling intervals (smooth curve). Superimposed to the condition number is the indicator function for the values allowed by the alias-free condition (4) (square waveform; the height of the pulses has no meaning).

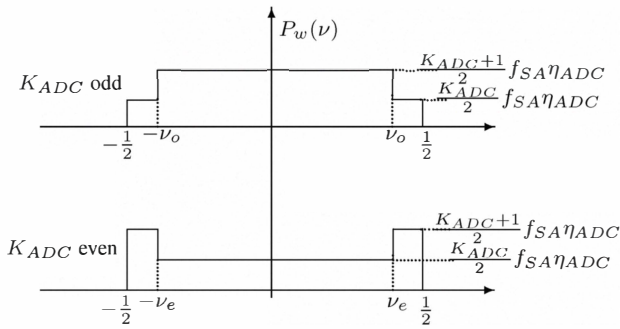


Fig. 5. Noise Power Spectral Density at the output of the ADC with analog bandwidth W_{ADC} and sampling rate f_{SA} for odd and even decimation factor K_{ADC} .

The optimal solution to recover the symbols in \mathbf{s} is the Maximum Likelihood (ML) receiver

$$\hat{\mathbf{s}}_{ML} = \arg \max_{\mathbf{s}} e^{-\frac{1}{2\sigma_w^2} \|\mathbf{y} - \mathbf{C}\mathbf{s}\|^2} = \arg \min_{\mathbf{s}} \|\mathbf{y} - \mathbf{C}\mathbf{s}\|^2. \quad (11)$$

Despite the simple formulation, the ML solution has exponential complexity [16] and can be applied directly only to low-dimensional problems. Alternatively, many sub-optimal receivers have been proposed in the literature, the most common being the Minimum Mean Square Error (MMSE) receiver [16] based on the linear estimate

$$\hat{\mathbf{s}}_{MMSE} = \mathbf{C}^T \left(\mathbf{C}\mathbf{C}^T + \frac{\sigma_w^2}{\sigma_s^2} \mathbf{I}_N \right)^{-1} \mathbf{y} \quad (12)$$

and on separate decisions on each component. The expression is derived under the assumption of symmetric and separable constellations, so that $E[\mathbf{s}] = \mathbf{0}$ and $E[\mathbf{s}\mathbf{s}^T] = \sigma_s^2 \mathbf{I}_M$. The error covariance on the symbols is

$$COV[\mathbf{s} - \mathbf{s}_{MMSE}] = \sigma_s^2 \left[\mathbf{I}_M - \mathbf{C}^T \left(\mathbf{C}\mathbf{C}^T + \frac{\sigma_w^2}{\sigma_s^2} \mathbf{I}_N \right)^{-1} \mathbf{C} \right].$$

Note that for a fixed number of symbols, by changing the sampling rate, we change also N , i.e. the row-dimension of \mathbf{C} and the

noise variance, because the decimation factor changes. Note also that, even though in the MMSE solution the matrix inversion in Eq. (12) is always possible because of the channel and the device noise, the choice of the sampling rate will affect symbol recovery because some symbols are canceled out if there is aliasing.

4. SIMULATIONS

In this section we present some simulations to check what happens in the signal recovery when a wrong sampling rate is chosen in our receiver. Our results confirm that for sampling periods that do not satisfy the alias-free conditions, poor performances are obtained because the reconstructing matrix becomes ill-conditioned. Fig. 6 shows BER as a function of SNR from a simulation with the 4-QAM signal of Fig. 3 with $L = 8$, $L_e = 4$, averaged over 3000 realizations with the ML and MMSE receivers. We have compared the receiver performance with sampling rate chosen according to Nyquist criterion and to the subsampling condition. Note that the “good” sampling interval is larger than the “bad” one, confirming that worse performance is not related to the problem order, but to proper sampling rate selection. When the alias-free condition is satisfied, MMSE and ML performance curves are essentially indistinguishable and they coincide with those obtained with Nyquist sampling rate. In the shown curves we do not explicitly account for the ADC noise because σ_{ADC}^2 strongly depends on the ADC technology. Since the noise contribution from the ADC can be assumed to be white, the receiver designer, once he knows about η_{ADC} and the decimation factor K_{ADC} , can account for the new SNR $\frac{\sigma_s^2}{\sigma_g^2 + \sigma_{ADC}^2} = \frac{\sigma_s^2}{\sigma_g^2} \frac{1}{1 + \frac{\sigma_{ADC}^2}{\sigma_g^2}}$, by shifting his design point in the per-

formance curve towards the left of $\Delta_{ADC} = 10 \log_{10} \left(1 + \frac{\sigma_{ADC}^2}{\sigma_g^2} \right)$. The performances presented here are typical of the many simulations we ran for various types of signals and problem orders. We have also investigated cases in which the signals are not exactly bandlimited. We found the alias-free criterion quite robust with respect to approximate or imperfect knowledge of the bands.

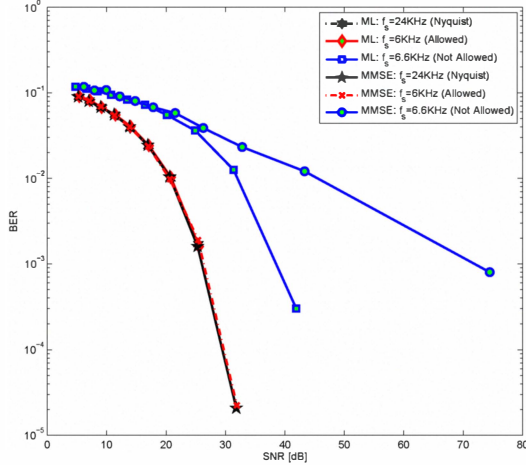


Fig. 6. Bit-Error Rate for a simulation with the ML and the MMSE receivers with three different sampling frequencies.

APPENDIX: Proof of Eq. (4): The elements of matrix $\mathbf{C}^T \mathbf{C}$ for N sufficiently large are of the type

$$\begin{aligned} & \sum_n \psi_a(nT_{SA} + t_0; i) \psi_b(nT_{SA} + t_0; j) = \\ & \sum_n \int \int \Psi_a(\xi; i) \Psi_b^*(\eta; j) e^{j2\pi(\xi-\eta)(nT_{SA} + t_0)} d\xi d\eta = \\ & \int \int \Psi_a(\xi; i) \Psi_b^*(\eta; j) e^{j2\pi(\xi-\eta)t_0} \frac{1}{T_{SA}} \sum_n \delta(\xi - \eta - \frac{n}{T_{SA}}) d\xi d\eta = \\ & \frac{1}{T_{SA}} \sum_n e^{j2\pi t_0 \frac{n}{T_{SA}}} \int \Psi_a(f; i) \Psi_b^*(f - \frac{n}{T_{SA}}; j) df, \quad (13) \end{aligned}$$

where the pair (a, b) is (c, c) , or (s, s) , or (c, s) , or (s, c) , and $\Psi_a(f; i)$ and $\Psi_b(f; j)$ are the Fourier transforms of $\psi_a(t; i)$ and $\psi_b(t; j)$ respectively. Expression (13) is periodic in t_0 and if

$$\begin{aligned} & \int \Psi_a(f; i) \Psi_b^*(f - \frac{n}{T_{SA}}; i) df = \\ & \mathcal{F} [\psi_a(t; i) \psi_b(t; j)]|_{f=nT_{SA}} = 0, \quad (14) \end{aligned}$$

for $n \neq 0$, we have the equivalence between discrete and continuous-time energies

$$\begin{aligned} & \sum_n \psi_a(nT_{SA} + t_0; i) \psi_b(nT_{SA} + t_0; j) = \\ & = \frac{1}{T_{SA}} \int \Psi_a(f; i) \Psi_b^*(f; j) df. \quad (15) \end{aligned}$$

Eq. (14) is our general *alias-free* condition. When Eq. (14) is satisfied for any pair (a, b) we have equivalence between the continuous-time and the discrete-time linear model. More specifically, consider any pair of modulating symbol vectors \mathbf{s} and \mathbf{u} . The square distance between the modulated analog signals is

$$\begin{aligned} d_c^2 &= \int ([\mathbf{z}(t)|\mathbf{s}] - [\mathbf{z}(t)|\mathbf{u}])^2 dt = \\ & \mathbf{s}^T R_c \mathbf{s} + \mathbf{u}^T R_c \mathbf{u} - 2\mathbf{s}^T R_c \mathbf{u}, \quad (16) \end{aligned}$$

where matrix R_c contains all the cross-products $\int \psi_a(t; i) \psi_b(t; j) dt$. The square distance between the sampled versions is

$$\begin{aligned} d^2 &= \|[\mathbf{z}|\mathbf{s}] - [\mathbf{z}|\mathbf{u}]\|^2 = \\ & \mathbf{s}^T \mathbf{C}^T \mathbf{C} \mathbf{s} + \mathbf{u}^T \mathbf{C}^T \mathbf{C} \mathbf{u} - 2\mathbf{s}^T \mathbf{C}^T \mathbf{C} \mathbf{u}. \quad (17) \end{aligned}$$

If the alias-free condition in Eq.(14) is satisfied, we have

$$\mathbf{C}^T \mathbf{C} = \frac{1}{T_{SA}} R_c; \quad d^2 = \frac{1}{T_{SA}} d_c^2, \quad (18)$$

i.e. after sampling, in the new vector space the symbol topology does not change. The noise variance scales similarly and we have complete equivalence between the optimal analog and discrete receivers. In our QAM signal $\psi_c(t; i)$ and $\psi_s(t; i)$ are bandlimited and the dependence on i does not change the band. The general condition in Eq.(14) simplifies to

$$\mathcal{F} [|\psi_c(t)|^2]|_{f=nT_{SA}} = 0, \quad \mathcal{F} [|\psi_s(t)|^2]|_{f=nT_{SA}} = 0, \quad n \neq 0,$$

or Eq. (4).

5. REFERENCES

- [1] E. Buracchini, CSELT, "The Software Radio Concept," *IEEE Communications Magazine*, vol. 38, no. 9, pp. 138-143, 2000.
- [2] J. Mitola, "The Software Radio Architecture," *IEEE Communications Magazine*, pp. 26-38, May 1995.
- [3] fred harris, "Software Defined Radio: A Tutorial," *IEEE Instrumentation and Measurement Magazine*, February 2010.
- [4] Rodney G.Vaughan, Neil L.Scott, and D. Rod White, "The Theory of Bandpass Sampling," *IEEE Transaction on Signal Processing*, vol. 39, no. 9, pp. 1973-1984, september 1991.
- [5] Y. C. Eldar, T. Michaeli, "Beyond Bandlimited Sampling: A Review of Nonlinearities, Smoothness and Sparsity," *IEEE Signal Proc. Magazine*, vol. 26, no. 3, pp. 48-68, May 2009.
- [6] D.A. Linden, "A Discussion of Sampling Theorem," *Proceedings of the IRE*, vol. 47, pp. 1219-1226, july 1959.
- [7] H. Landau, "Sampling, Data Transmission and the Nyquist Rate," *Proc. of IEEE*, vol 65, no. 10, pp. 1701-1706, 1967.
- [8] M. Unser, "Sampling-50 Years After Shannon," *Proc. of IEEE*, vol 88, no. 4, pp. 569-587, april 2000.
- [9] B. Le, T.W. Rondeau, J.H. Reed, C.W. Bostian, "Analog-to-Digital Converters: a Review of the Past, Present and Future," *IEEE Signal Processing Magazine*, vol 22, no. 6, pp. 69-77, november 2005.
- [10] R.H. Walden, "Analog-to-Digital Converter Survey and Analysis," *IEEE Journal on Selected Areas in Communications*, vol 17, no. 4, april 1999.
- [11] Y.S. Poberezhskiy, "A New Approach to Increasing Sensitivity and Resolution of A/Ds," *Proceedings of 2009 IEEE Aerospace Conference*, March 7-14, 2009, Big Sky, Montana.
- [12] Y.S. Poberezhskiy, G.Y. Poberezhskiy "Some Aspects of Design of Software Defined Receivers Based on Sampling with Internal Filtering," *Proceedings of 2009 IEEE Aerospace Conference*, March 7-14, 2009, Big Sky, Montana.
- [13] Y. M. Lu, M. N. Do, and R. S. Laugesen, "A Computable Fourier Condition Generating Alias-Free Sampling Lattices," *IEEE Transactions on Signal Processing*, vol. 57, N. 5, pp. 1768-1782, May 2009.
- [14] F. Xiong, *Digital Modulation Techniques*, Artech House telecommunications library, 685 Canton Street, Norwood, MA 02062.
- [15] F. Palmieri, E. Venosa, G. Romano, P. Salvo Rossi and A. Petropulu, "On Low-Rate Sampling for Digital Communication Signals," submitted to *IEEE Trans. on Signal Processing*, Jan 2010 (manuscript available on request).
- [16] E. Biglieri, R. Calderbank, A. Constantinides, A. Goldsmith, A. Paulraj, H. Vincent Poor, *MIMO Wireless Communications*, Cambridge University Press 2007.